Nonlinear topological edge states in a non-Hermitian array of optical waveguides embedded in an atomic gas

Chao Hang,[1,2] Dmitry A. Zezyulin,[3] Guoxiang Huang,[1,2] and Vladimir V. Konotop[4,5]

[1]*State Key Laboratory of Precision Spectroscopy, East China Normal University, Shanghai 200062, China*
[2]*NYU-ECNU Institute of Physics at NYU-Shanghai, Shanghai 200062, China*
[3]*ITMO University, St. Petersburg 197101, Russia*
[4]*Departamento de Física, Faculdade de Ciências, Universidade de Lisboa,
Campo Grande, Edifício C8, Lisboa 1749-016, Portugal*
[5]*Centro de Física Teórica e Computacional, Faculdade de Ciências, Universidade de Lisboa,
Campo Grande, Edifício C8, Lisboa 1749-016, Portugal*

We propose a scheme comprising an array of anisotropic optical waveguides, embedded in a gas of cold atoms, which can be tuned from a Hermitian to an odd-$\mathcal{PT}$-symmetric configuration through the manipulation of control and assistant laser fields. We show that the system can be controlled by tuning intra- and intercell coupling coefficients, enabling the creation of topologically distinct phases and linear topological edge states. The waveguide array, characterized by a quadrimer primitive cell, allows for implementing transitions between Hermitian and odd-$\mathcal{PT}$-symmetric configurations, broken and unbroken $\mathcal{PT}$-symmetric phases, topologically trivial and nontrivial phases, as well as transitions between linear and nonlinear regimes. The introduced scheme generalizes the Rice-Mele Hamiltonian for a nonlinear non-Hermitian quadrimer array featuring odd-$\mathcal{PT}$ symmetry and makes accessible unique phenomena and functionalities that emerge from the interplay of non-Hermiticity, topology, and nonlinearity. We also show that in the presence of nonlinearity the system sustains nonlinear topological edge states bifurcating from the linear topological edge states and the modes without a linear limit. Each nonlinear mode represents a doublet of odd-$\mathcal{PT}$-conjugate states. In the broken $\mathcal{PT}$ phase, the nonlinear edge states may be effectively stabilized when an additional absorption is introduced into the system.

Introduction. Optical systems are universal simulators of physical phenomena from many areas of physics. In the past decade particular attention was focused on optical analogs of topological insulators, having fundamental importance for condensed-matter physics [1,2]. Pioneered by the works [3,4], a new field of topological photonics [5,6] has emerged. Non-Hermitian topological insulators were established to have two different types of phase transitions, i.e., the transitions between pure real and complex spectra of linear Hamiltonians [7,8] and between topologically distinct phases [5,6]. Topological properties of linear non-Hermitian systems are now well understood, and their classifications based on the symmetries of systems are available [9,10]. It is also known that in a finite non-Hermitian system with boundaries, edge states can be sustained by nontrivial topological phases [5,6]. Linear edge states at the interface between $\mathcal{PT}$-symmetric Su-Schrieffer-Heeger (SSH) [11] photonic lattices in distinct topological phases have been observed experimentally [12]. Topological zero-energy edge states in passive-$\mathcal{PT}$ silicon waveguide arrays [13] have been reported, too.

In optical settings, topological phenomena are further enriched by nonlinearity [14]. Nontopological nonlinear parity ($\mathcal{P}$)-time ($\mathcal{T}$) symmetric systems [15,16] may sustain families of nonlinear modes without linear counterparts [17]. Meantime, not every linear mode persists in the presence

of nonlinearity, i.e., the nonlinearity must obey the symmetry consistent with that of the linear system in order to enable a bifurcation of a nonlinear family from the linear limit [17,18]. Nonlinearity may also result in $\mathcal{PT}$-symmetry breaking [19,20], in pitchfork symmetry-breaking bifurcations [21], and in destabilizing (stabilizing) a linear mode which is otherwise stable (unstable) [22]. Self-induced topological transitions and edge states have been reported in nonlinear SSH arrays [23]. Nonlinear topological edge modes were created in an array of pumped resonators [24].

However, so far nonlinear modes in non-Hermitian systems have been considered mainly under even-$\mathcal{PT}$ symmetry, for which $\mathcal{T}^2 = 1$ [15,16]. It was shown that the realization of *odd* time reversal (for which $\mathcal{T}^2 = -1$) is available [25,26] by using the polarization of light in waveguides with anti-$\mathcal{PT}$-symmetric [27,28] coupling. The major difference between the even- and odd-$\mathcal{PT}$-symmetric lattices consists in their elementary cells: A primitive cell of an even-$\mathcal{PT}$-symmetric chain is a dimer [15,16,29] whereas that of an odd-$\mathcal{PT}$-symmetric lattice is a quadrimer [25] (in analogy with the structures of wave functions of even- and odd-$\mathcal{PT}$-symmetric quantum Hamiltonians [30,31]). Particularly, guided modes in odd-$\mathcal{PT}$-coupler waveguides feature intrinsic symmetry-protected degeneracy which allows one to manipulate superpositions of degenerate modes and results in unconventional bifurcations of nonlinear states [25].
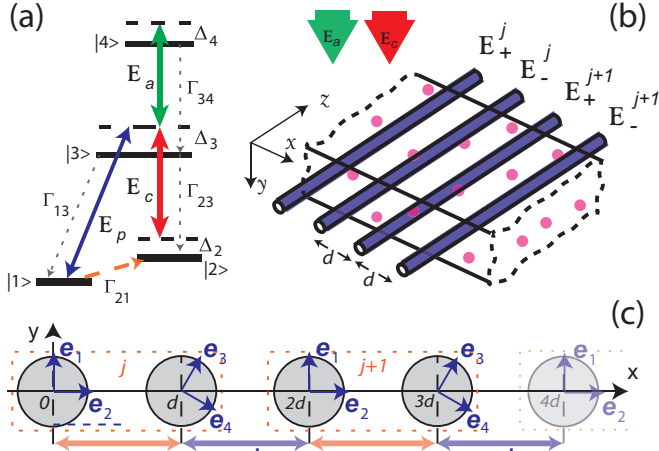
FIG. 1. (a) The energy-level diagram and the excitation scheme of the inverted-Y-type system. The probe ($\mathbf{E}_p$), control ($\mathbf{E}_c$), and assistant ($\mathbf{E}_a$) laser fields drive transitions $|1\rangle \leftrightarrow |3\rangle$, $|2\rangle \leftrightarrow |3\rangle$, and $|3\rangle \leftrightarrow |4\rangle$, respectively. Γ_{21} denotes the incoherent pumping rate from $|1\rangle$ to $|2\rangle$ (providing gain); other Γ_{jl} are spontaneous-emission decay rates from $|j\rangle$ to $|l\rangle$. (b) A possible setup for realizing the target probe-field susceptibility consisting of an array of optical waveguides, equally separated by distance d, embedded in the atomic gas. (c) Polarizations and primitive cells j and $j+1$ (shown by dotted lines) of an array with intra- and intercell coupling coefficients κ and κ'.

The goal of this Letter is twofold. First, we propose a versatile system, i.e., an array of optical waveguides embedded in an atomic gas, that allows one to combine different physical phenomena in a manageable manner, including topological phase transitions, spontaneous $\mathcal{PT}$-symmetry breaking, and nonlinearity in a nonlinear quadrimer system featuring odd-$\mathcal{PT}$ symmetry. Second, we introduce a nonlinear non-Hermitian quadrimer generalization of the well-known Rice-Mele model [32], that describes the above array, report families of nonlinear modes bifurcating from linear topological edge states, and study the stability of nonlinear edge states. We show that each of the degenerated linear modes bifurcates in two distinct nonlinear families, and each nonlinear mode represents a doublet of odd-$\mathcal{PT}$-conjugate states. The modes in the doublet share the same propagation constant and power but have different field polarizations. The doublet families generated at the left and right edges are characterized by different existence ranges and stability properties. The findings reported here bring insights to the interplay of non-Hermiticity, topology, and nonlinearity for realizing different phase transitions and nonlinear modes in a universal platform and achieving their active manipulation, promising for applications in optical information processing and transmission.

The physical model. A dielectric permittivity of an atomic gas can be modified with great flexibility allowing for the creation of a prescribed symmetry [33–36]. Bearing this in mind, we consider an array of anisotropic optical waveguides, having equal radii r_w, embedded in a cold four-level atomic gas with an inverted-Y-type configuration [Fig. 1(a)]. The use of the inverted-Y configuration is to take the advantage of electromagnetically induced transparency [37], which can

largely suppress the large absorption of the probe field due to the spontaneous emission of the atoms in the intermediated state $|3\rangle$; additionally, it is useful for realizing the odd-$\mathcal{PT}$ symmetry in the system by tuning the control and assistant fields independently.

Neighboring waveguides are separated by a distance d [Fig. 1(b)] and are arranged to have their principal optical axes mutually rotated in the (x, y) plane by an angle α [Fig. 1(c)]. The principal optical axes of a pair of waveguides in a primitive cell are determined by two pairs of mutually orthogonal unit vectors $\mathbf{e}_{1,2}$ and $\mathbf{e}_{3,4}$, corresponding to the left and right waveguides in a cell. The waveguides have equal x and y components of the dielectric tensor but different z components, originating a mismatch 2δ between the propagation constants of the left ("+") and right ("−") waveguides, i.e., $\beta_\pm = \beta \pm \delta$ (β is the average propagation constant).

We apply control (c) and assistant (a) fields $E_s = \mathcal{E}_s e^{ik_s y - i\omega_s t} + \text{c.c.}$ (hereafter $s = a, c$) to the atomic cell [Fig. 1(b)]. A transversely polarized probe laser field is applied to the waveguides, generating guided modes with mutually orthogonal linear polarizations, holding also outside the waveguides due to weak guidance. The components of the probe field in the jth primitive cell can be expressed as

$$\mathbf{E}_{+,-}^j = \left(\mathbf{e}_{1,3} A_{1,3}^j \psi_{1,3}^j + \mathbf{e}_{2,4} A_{2,4}^j \psi_{2,4}^j\right) e^{i\beta_\pm z - i\omega_p t}, \quad (1)$$

where $A_{1,\dots,4}^j(z)$ are slowly varying amplitudes, and $\psi_{1,\dots,4}^j(\mathbf{r})$ are normalized transverse distributions.

Under electric-dipole and rotating-wave approximations, the system Hamiltonian in the interaction picture reads $\hat{H}_{\text{int}} = \hbar \sum_{j=2}^4 [\Delta_j |j\rangle\langle j| - \hbar(\Omega_p |3\rangle\langle 1| + \Omega_c |3\rangle\langle 2| + \Omega_a |4\rangle\langle 3| + \text{H.c.})]$. Here, Δ_j are detunings, and $\Omega_p = (\mathbf{e}_z \cdot \mathbf{p}_{31})\mathcal{E}_p/\hbar$, $\Omega_c = (\mathbf{e}_z \cdot \mathbf{p}_{32})\mathcal{E}_c/\hbar$, and $\Omega_a = (\mathbf{e}_z \cdot \mathbf{p}_{43})\mathcal{E}_a/\hbar$ are respectively Rabi frequencies of the probe, control, and assistant fields, with $\mathbf{p}_{jl}$ being the electric-dipole matrix elements associated with the transition between the atomic states $|j\rangle$ and $|l\rangle$. The dephasing due to the interaction of atoms near the waveguide surfaces may be avoided by using a coating paraffin or siloxane on the surfaces [38], or by using the technique of a nanofiber-based optical dipole trap [39]. The probe-field susceptibility χ_p can be obtained by solving the Maxwell-Bloch equations governing the evolution of the atoms and the light field (see Supplemental Material [40] for details).

Our target is to acquire an x-dependent probe-field susceptibility $\chi_p(x)$ which under the change of the parameters leads either to a Hermitian or to a $\mathcal{PT}$-symmetric array. In particular, one obtains [40]

$$\chi_p = \chi_w + i\chi_i - e^{i\phi_1} \chi_1 \cos(2\pi x/d) - e^{i\phi_2} \chi_2 \sin(\pi x/d), \quad (2)$$

where χ_w is a real transverse susceptibility of a waveguide, χ_i describes uniform gain or absorption, and $\chi_{1,2}$ ($|\chi_{1,2}| \ll |\chi_w|$) and $\phi_{1,2}$ are respectively amplitudes and phases of the susceptibility modulations. The distribution (2) can be achieved, e.g., in a gas of laser-cooled ^{87}Rb atoms with the levels assigned as $|1\rangle = |5S_{1/2}, F = 1\rangle$, $|2\rangle = |5S_{1/2}, F = 2\rangle$, $|3\rangle = |5P_{3/2}, F = 3\rangle$, $|4\rangle = |6S_{1/2}\rangle$, with the atomic parameters given by $\mathcal{N}_a = 3.0 \times 10^{14}$ cm^{-3} (atomic density), $\Gamma_{13} \approx \Gamma_{23} \approx 10^3 \Gamma_{34} \approx 2\pi \times 3$ MHz, $\Gamma_{21} \approx 2\pi \times 50$ kHz, $\Delta_2 = 0.1$ MHz, $\Delta_3 = -41$ MHz, and $\Delta_4 = 0.2$ GHz.

To obtain susceptibility (2) in this system the Rabi frequencies must satisfy [40]

$$\Omega_s \approx \Omega_{s0} + \Omega_{s1}\chi_1 \cos(\phi_1 + \phi_s)\cos(2\pi x/d)$$
$$+ \Omega_{s1}\chi_2 \cos(\phi_2 + \phi_s)\sin(\pi x/d), \quad (3)$$

where $\Omega_{c0} = 10$ MHz, $\Omega_{a0} = 20$ MHz, $\Omega_{c1} \approx 8$ MHz, $\Omega_{a1} \approx 610$ MHz, $\phi_c \approx 1.1$, and $\phi_a \approx -0.3$ ($\chi_{1,2}$ and $\phi_{1,2}$ remain to be free parameters). The validity of susceptibility (2) should be limited to a certain domain, say for an array of 20 waveguides with $d = 4r_w = 4$ μm.

A non-Hermitian nonlinear quadrimer lattice. For cylindrical waveguides in the tight-binding approximation one has $\psi_{1,2}^{(j)}(\mathbf{r}) \approx \psi(\mathbf{r})$ and $\psi_{3,4}^{(j)}(\mathbf{r}) \approx \psi(x - d, y)$. The probe field in the array [Figs. 1(b) and 1(c)] is governed by the equation for the amplitude column vector $\mathbf{A}^j = (A_1^j, A_2^j, A_3^j, A_4^j)^{\mathrm{T}}$ (T means transposition),

$$i\frac{d\mathbf{A}^j}{dz} = H\mathbf{A}^j + \kappa'(H_-\mathbf{A}^{j-1} + H_+\mathbf{A}^{j+1}) - F(\mathbf{A}^j)\mathbf{A}^j. \quad (4)$$

Here, $H = \delta\sigma_3 \otimes \sigma_0 + \kappa(H_+ + H_-)$, $\sigma_{1,2,3}$ are the Pauli matrices, σ_0 is the 2×2 identity matrix, $H_- = H_+^{\mathrm{T}} = \frac{i}{2}(\sigma_1 + i\sigma_2) \otimes \mathrm{R}_\alpha$, and R_α is the matrix of two-dimensional rotation by the angle α. The intracell (κ) and intercell (κ') coupling coefficients are given by [40]

$$\{\kappa, \kappa'\} = \frac{k_p}{2i} \int_{jd}^{(j+1)d} dx \int_{-\infty}^{\infty} dy\, \psi(\sqrt{x^2 + y^2})$$
$$\times [\chi_w - \chi_p(x - jd)]\psi(\sqrt{(x-d)^2 + y^2}), \quad (5)$$

where $j = 0$ ($j = 1$) stands for κ (κ'). The diagonal focusing Kerr nonlinearity matrix reads

$$F(\mathbf{A}^j) = \mathrm{diag}\left(\left|A_1^j\right|^2 + \frac{2}{3}\left|A_2^j\right|^2, \left|A_2^j\right|^2 + \frac{2}{3}\left|A_1^j\right|^2,\right.$$
$$\left.\left|A_3^j\right|^2 + \frac{2}{3}\left|A_4^j\right|^2, \left|A_4^j\right|^2 + \frac{2}{3}\left|A_3^j\right|^2\right). \quad (6)$$

By changing the parameters $\chi_{1,2}$ and $\phi_{1,2}$ one can obtain different symmetries and phases of the chain (4). In particular, if $(\phi_1, \phi_2) = (\pi/2, \pm\pi/2)$ and $\chi_i = 0$ in (2), κ and κ' are both real and the array is non-Hermitian; we call it an odd-$\mathcal{PT}$ chain. Such a chain features odd-$\mathcal{PT}_f$ symmetry [25,30,31] with the parity operator $\mathcal{P} = \sigma_3 \otimes \sigma_0$ and an odd-time-reversal (or fermionic) operator $\mathcal{T}_f = i\sigma_0 \otimes \sigma_2 \mathcal{K}$, with $\mathcal{K}$ being the complex conjugation ($\mathcal{T}_f^2 = -1$). If $\phi_1 = 0$ and $\phi_2 = 0, \pi$, then κ and κ' are both imaginary, and the array is Hermitian; we call it an h-chain. An h chain is $\mathcal{T}_f$ and $\mathcal{T}$ symmetric with $\mathcal{T} = \mathcal{K}$ ($\mathcal{T}^2 = 1$). Furthermore, one can obtain topologically trivial ($|\kappa| > |\kappa'|$) and topologically nontrivial ($|\kappa| < |\kappa'|$) phases by choosing, respectively, $\phi_2 = \pi/2$ ($\phi_2 = \pi$) and $\phi_2 = -\pi/2$ ($\phi_2 = 0$) for an odd-$\mathcal{PT}$ chain (h-chain). Without loss of generality, we assume $\delta \geqslant 0$, and $\kappa, \kappa' \geqslant 0$ (for odd-$\mathcal{PT}$ chain) and $\mathrm{Im}\,\kappa$, $\mathrm{Im}\,\kappa' \geqslant 0$ (for h-chain).

The relation between the parameters of the gas and different topological phases follows from the fact that the linear Hamiltonian of (4) [at $F(\mathbf{A}^j) = 0$] in the momentum space ($\mathbf{A}^j = \mathbf{a}_q e^{iqj}$), $H(q)$, can be block-diagonalized by the unitary transformation

$$UH(q)U^\dagger = \sigma_0 \otimes h(q), \quad U = \begin{pmatrix} -\sin\alpha & \cos\alpha & 0 & 0 \\ 0 & 0 & 0 & 1 \\ \cos\alpha & \sin\alpha & 0 & 0 \\ 0 & 0 & 1 & 0 \end{pmatrix},$$

where $h(q) = i(\kappa + \kappa'\cos q)\sigma_1 + i\kappa'\sin(q)\sigma_2 + \delta\sigma_3$. In the Hermitian case, $h(q)$ is the celebrated Rice-Mele Hamiltonian [32,49] whose non-Hermitian generalization is also known [50]. Thus, Eq. (4) can be viewed as a *nonlinear non-Hermitian quadrimer generalization of the Rice-Mele model*, where $A_{1,\dots,4}^j$ can be treated as "internal" degrees of freedom of the jth primitive cell. Topological properties of the linear limit of (4) are determined by the topological properties of $h(q)$. Indeed, let $\mathbf{a}_q$ and $\tilde{\mathbf{a}}_q$ be the eigenvectors of $H(q)$ and $H^\dagger(q)$ constituting a biorthonormal basis ($\tilde{\mathbf{a}}_{q'}^\dagger \mathbf{a}_q = \delta_{q'q}$; hereafter δ_{mj} is the Kronecker symbol), and the Zak phase for a given band is defined by $\varphi = \int_{\mathrm{BZ}} \tilde{\mathbf{a}}_q^\dagger \partial_q \mathbf{a}_q dq$, where the integral is over the Brillouin zone. Let also $\boldsymbol{\alpha}_q$ and $\tilde{\boldsymbol{\alpha}}_q$ be the eigenvectors of $h(q)$ and $h^\dagger(q)$ constituting a biorthonormal basis ($\tilde{\boldsymbol{\alpha}}_{q'}^\dagger \boldsymbol{\alpha}_q = \delta_{q'q}$), while $\varphi_h = \int_{\mathrm{BZ}} \tilde{\boldsymbol{\alpha}}_q^\dagger \partial_q \boldsymbol{\alpha}_q dq$ is the Zak phase of the Rice-Mele lattice defined by $h(q)$. Then the block-diagonal structure of $UH(q)U^\dagger$ implies that $\mathbf{a}_q = (1, 1)^{\mathrm{T}} \otimes \boldsymbol{\alpha}_q/\sqrt{2}$ and, respectively, $\varphi = \varphi_h$. The phases φ_h are computed explicitly in the Supplemental Material [40].

Eigenvalues of the linear limits of both the h-chain and odd-$\mathcal{PT}$ chain are doubly degenerate: There are two branches of bulk modes $\pm\tilde{b}(q)$, where $\tilde{b}(q) = [\delta^2 - \kappa^2 - \kappa'^2 - 2\kappa\kappa'\cos q]^{1/2}$. An odd-$\mathcal{PT}$ chain can belong to an unbroken ($\delta > \delta_1 \equiv \kappa + \kappa'$), *partially* broken ($\delta_2 \equiv |\kappa - \kappa'| < \delta < \delta_1$), or *fully* broken ($\delta < \delta_2$) phase. Since $\tilde{b}(q) = \tilde{b}(-q)$, in the case at hand the skin effect [51,52] is prevented by the symmetry [10] (which does not exclude that effect subject to different properties of the quadrimers obtained by proper configurations of the external fields).

Nonlinear edge states. Semi-infinite chains are obtained by the truncation of (4). For the left-edge ("L") chain we consider $\mathbf{A}_L^{0,1,\dots}$ assuming $\mathbf{A}_L^{-1} = 0$. For the right-edge ("R") chain we consider $\mathbf{A}_R^{0,-1,\dots}$ assuming $\mathbf{A}_R^1 = 0$. In the linear limit of the topologically nontrivial phase, $|\kappa/\kappa'| < 1$, at each edge there exist two independent edge states: $\mathbf{A}_{L,m}^j = (-\kappa/\kappa')^j e^{-i\delta z}(\delta_{m1}, \delta_{m2}, 0, 0)^{\mathrm{T}}$ and $\mathbf{A}_{R,m}^j = (-\kappa'/\kappa)^j e^{i\delta z}(0, 0, \delta_{m1}, \delta_{m2})^{\mathrm{T}}$, with $m = 1, 2$.

Nontrivial topology by itself is not necessary for the existence of nonlinear edge states [53,54]. Meantime, nonlinear modes can bifurcate from the linear topological edge states $\mathbf{A}_{L,m}^j$ and $\mathbf{A}_{R,m}^j$, when topological characteristics of the bifurcating families are uniquely associated with the topological numbers of the underlying linear lattice. Such modes will be called *nonlinear topological edge states*. Below we focus on the families of solutions in the odd-$\mathcal{PT}$ chain. Owing to the odd-$\mathcal{PT}$-symmetry-protected degeneracy of guided modes, in the small-amplitude limit, nonlinear edge states can be searched as a superposition: $\mathbf{A}_g^j \approx \epsilon e^{i\epsilon^2\lambda z}(\mathbf{A}_{g;1}^j \sin\nu + \mathbf{A}_{g;2}^j \cos\nu)$, where $g = L$ (L modes) or $g = R$ (R modes), $\epsilon \ll 1$ is a formal small parameter, λ is the nonlinearity-induced shift of the propagation constant, and ν is a parameter to be determined. The perturbation analysis [18,25,40,55] reveals
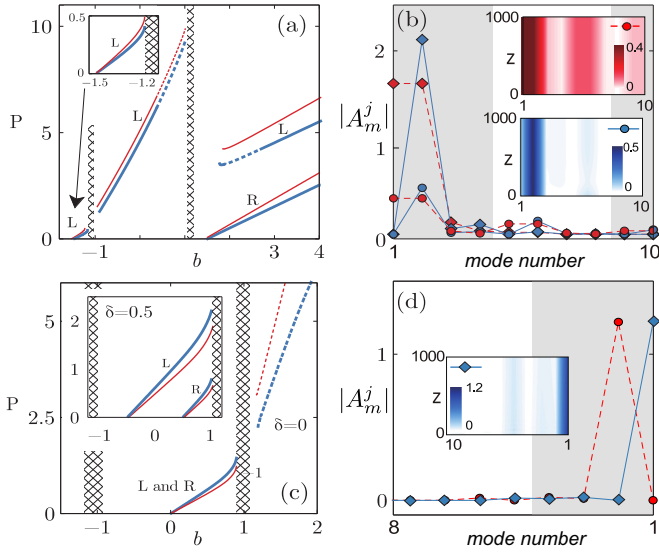
FIG. 2. (a) Families of nonlinear edge states in the odd-$\mathcal{PT}$ chain with unbroken $\mathcal{PT}$ symmetry for $(\kappa, \kappa') = (0.1, 1)$ and $\delta = 1.5$. Hatched areas indicate the spectral bands. The blue thick and red thin lines correspond to $\nu = 0$ and $\nu = \pi/4$, respectively. Solid and dashed curve fragments correspond to stable and unstable edge states. The inset zooms in families bifurcating from the left linear edge states. (b) Examples of L modes in the lower semi-infinite gap with $b = -1.25$ (blue solid and red dashed lines with circles) and in the upper semi-infinite gap with $b = 3$ (blue solid and red dashed lines with diamonds); the lower and upper insets show respectively stable propagation of L modes in blue solid and red dashed lines with circles. (c) Families of nonlinear edge states in the h-chain for $(\kappa, \kappa') = (0.1i, i)$ and $\delta = 0$ (main panel) or $\delta = 0.5$ (inset). (d) Example of the R mode in the odd-$\mathcal{PT}$ chain with $b = 3$ (blue solid line with diamonds), and its $\mathcal{PT}_f$ partner (red dashed line with circles); the inset illustrates the stable propagation of the R mode in the blue solid line with diamonds. In all panels $\alpha = \pi/6$.

two cases when the bifurcations are allowed. In the first case $\nu = \pi/4$, i.e., the bifurcation occurs from the linear superposition of two states $\boldsymbol{A}_{g,1}$ and $\boldsymbol{A}_{g,2}$ with equal "weights," and $\lambda = 5\kappa'^2/[6(\kappa'^2 + \kappa^2)]$. In the second case $\nu = 0$, i.e., the nonlinear mode bifurcates from only one linear edge state and $\lambda = \kappa'^2/(\kappa'^2 + \kappa^2)$.

The above small-amplitude edge states serve as an initial guess for the numerical investigation of entire families of stationary nonlinear edge states whose dependence on z is $A_g^j(z) \propto e^{ibz}$, where b is the real nonlinear propagation constant. Distinct families are characterized by the dependencies of the total dimensionless power $P_g = \sum (A_g^j)^\dagger A_g^j$ on b.

In the unbroken $\mathcal{PT}$-symmetric phase ($\delta > \delta_1$), the linear spectrum of (4) consists of two bands separated by a central finite gap [Fig. 2(a)]. In the topologically nontrivial phase there exist two linear edge states in the semi-infinite gaps. The families of L and R modes bifurcate from the linear edge states in the lower and upper semi-infinite gaps, respectively. There also exist families of nonlinear edge states having nonzero excitation power threshold, as illustrated in Fig. 2(a). L modes exist only in a relatively narrow interval of b between $-\delta$ and the lower edge of the first band. These modes become delocalized when they approach the first band and

"reappear" in the finite gap. Meanwhile, nonzero-threshold families of L modes exist also in the upper semi-infinite gap, where two zero-threshold families of R modes emerge in the upper semi-infinite gap. Using a linear stability analysis and direct propagation method, we find that all nonlinear modes shown in Fig. 2(a) are stable except for small segments plotted with dashed lines. In contrast to the more common even-$\mathcal{PT}$ symmetry with $\mathcal{T}^2 = 1$, the odd time reversal implies that any nonlinear edge state represents a *doublet*, i.e., the pair $(\boldsymbol{A}, \mathcal{PT}_f \boldsymbol{A})$, characterized by different polarizations of the fields $\boldsymbol{E}_\pm^j$ in Eq. (1). Remarkably, due to the symmetry both modes in each doublet are stable (or unstable) simultaneously.

For comparison, in Fig. 2(c) we show families of nonlinear edge states in an h-chain, where bifurcation occurs from edge states in the finite gap. For $\delta = 0$ (the quadrimer SSH limit) we observe families of doublets bifurcating from the zero-energy topological linear edge state. The degeneracy is lifted at $\delta \neq 0$ [inset in Fig. 2(c), where L and R modes have different power dependencies].

In Fig. 3(a) we show families bifurcating from linear topological edge states in the broken $\mathcal{PT}$-symmetric phase. These families behave similarly to those in the unbroken case, except that now there exists only one linear band due to the closing of the gap. In the fully broken $\mathcal{PT}$ phase ($\delta < \delta_2$) the families of the L modes are continuous [inset in Fig. 3(a)] since the linear band consists of purely imaginary propagation constants.

Unlike in the case of the unbroken $\mathcal{PT}$-symmetric phase where the instability is triggered only by nonlinearity, in the broken $\mathcal{PT}$-symmetric phases all nonlinear edge states are *a priori* unstable, because a continuum of unstable linear waves inevitably destabilizes the "tails" of edge states, as exemplified in Fig. 3(b1). Remarkably, even in a fully broken $\mathcal{PT}$ phase, nonlinear edge states can be almost stabilized by introducing additional absorption in the central part of the lattice. The introduction of such absorption (which is localized in the region of exponentially decaying tails of the edge
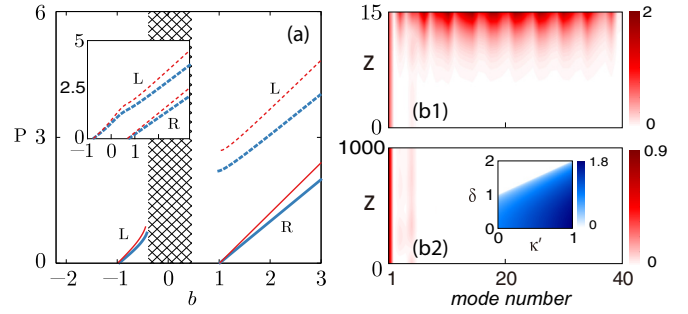

FIG. 3. (a) Families of nonlinear edge states in the partially broken odd-$\mathcal{PT}$ phase with $\delta = 1$; the inset shows the families in the fully broken $\mathcal{PT}$ phase with $\delta = 0.8$. The hatched area corresponds to the linear band. The blue thick and red thin lines correspond to $\nu = 0$ and $\nu = \pi/4$, respectively. (b1) Unstable propagation of the L mode in the partially broken $\mathcal{PT}$ phase. (b2) Quasistable propagation of the same mode as in (b1) but in the presence of additional absorption with $\gamma = 0.5$; the inset shows domains of unbroken (white) and broken (blue) $\mathcal{PT}$ phases in the (κ', δ) panel with $\kappa = 1$. The color bar shows the maximum of $\text{Im}[\tilde{b}_+(q)]$. Other parameters are the same as in Fig. 2(a).

states) aims to suppress the growth of unstable bulk modes but has no significant effect on the edge states themselves. This determines the strength of the absorption γ which must be equal to the largest increment of the bulk modes, characterized by the maximum of $\text{Im}[\tilde{b}_+(q)]$, i.e., $\gamma = \max(\text{Im}(\tilde{b}_+(q)))$. By introducing such absorption as an additional term $-i\gamma A^j$ on the right-hand side of Eq. (4), the L mode can propagate robustly up to $z = 1000$, as illustrated in Fig. 3(b2).

Conclusion. We have introduced a nonlinear non-Hermitian quadrimer generalization of the Rice-Mele model, with a primitive cell characterized by four degrees of freedom. The model describes an array of anisotropic waveguides embedded in a gas of cold atoms, and represents a universal platform for the implementation of several types of phase transitions in a single setting, as well as different symmetries in the nonlinear regime. Varying external laser fields enable transitions between Hermitian and non-Hermitian configurations, as well as between trivial and nontrivial topological phases, both in linear and nonlinear regimes. We have considered the cases when the chain is either Hermitian or non-Hermitian featuring odd-time-reversal symmetry, the latter supporting

doublets of nonlinear states. The modes in the doublet are characterized by different light polarizations but identical stability properties. Families of nonlinear topological modes are unambiguously related to the topological linear edge states they are bifurcating from. Even in the broken $\mathcal{PT}$-symmetric phase, the observation of nonlinear edge doublets is possible by using additional stabilizing absorption in the central part of the array.

[1] M. Z. Hasan and C. L. Kane, Topological insulators, Rev. Mod. Phys. **82**, 3045 (2010).

[2] X.-L. Qi and S.-C. Zhang, Topological insulators and superconductors, Rev. Mod. Phys. **83**, 1057 (2011).

[3] F. D. M. Haldane and S. Raghu, Possible Realization of Directional Optical Waveguides in Photonic Crystals with Broken Time-Reversal Symmetry, Phys. Rev. Lett. **100**, 013904 (2008).

[4] S. Raghu and F. D. M. Haldane, Analogs of quantum-Hall-effect edge states in photonic crystals, Phys. Rev. A **78**, 033834 (2008).

[5] L. Lu, J. D. Joannopoulos, and M. Soljačić, Topological photonics, Nat. Photonics **8**, 821 (2014).

[6] T. Ozawa, H. M. Price, A. Amo, N. Goldman, M. Hafezi, L. Lu, M. C. Rechtsman, D. Schuster, J. Simon, O. Zilberberg, and I. Carusotto, Topological photonics, Rev. Mod. Phys. **91**, 015006 (2019).

[7] C. M. Bender, Making sense of non-Hermitian Hamiltonians, Rep. Prog. Phys. **70**, 947 (2007).

[8] S. Boettcher and C. M. Bender, Real Spectra in Non-Hermitian Hamiltonians Having *PT* Symmetry, Phys. Rev. Lett. **80**, 5243 (1998).

[9] Z. Gong, Y. Ashida, K. Kawabata, K. Takasan, S. Higashikawa, and M. Ueda, Topological Phases of Non-Hermitian Systems, Phys. Rev. X **8**, 031079 (2018).

[10] K. Kawabata, K. Shiozaki, M. Ueda, and M. Sato, Symmetry and Topology in Non-Hermitian Physics, Phys. Rev. X **9**, 041015 (2019).

[11] W. P. Su, J. R. Schrieffer, and A. J. Heeger, Solitons in Polyacetylene, Phys. Rev. Lett. **42**, 1698 (1979).

[12] S. Weimann, M. Kremer, Y. Plotnik, Y. Lumer, S. Nolte, K. G. Makris, M. Segev, M. C. Rechtsman, and A. Szameit, Topologically protected bound states in photonic parity-time-symmetric crystals, Nat. Mater. **16**, 433 (2016).

[13] W. Song, W. Sun, C. Chen, Q. Song, S. Xiao, S. Zhu, and T. Li, Breakup and Recovery of Topological Zero Modes in Finite

Non-Hermitian Optical Lattices, Phys. Rev. Lett. **123**, 165701 (2019).

[14] D. Smirnova, D. Leykam, Y. Chong, and Y. Kivshar, Nonlinear topological photonics, Appl. Phys. Rev. **7**, 021306 (2020).

[15] V. V. Konotop, J. Yang, and D. A. Zezyulin, Nonlinear waves in $\mathcal{PT}$-symmetric systems, Rev. Mod. Phys. **88**, 035002 (2016).

[16] S. V. Suchkov, A. A. Sukhorukov, J. Huang, S. V. Dmitriev, C. Lee, and Y. S. Kivshar, Nonlinear switching and solitons in PT-symmetric photonic systems, Laser Photonics Rev. **10**, 177 (2016).

[17] D. A. Zezyulin and V. V. Konotop, Nonlinear Modes in Finite-Dimensional $\mathcal{PT}$-Symmetric Systems, Phys. Rev. Lett. **108**, 213906 (2012).

[18] D. A. Zezyulin and V. V. Konotop, Stationary modes and integrals of motion in nonlinear lattices with a $\mathcal{PT}$-symmetric linear part, J. Phys. A: Math. Theor. **46**, 415301 (2013).

[19] V. Achilleos, P. G. Kevrekidis, D. J. Frantzeskakis, and R. Carretero-González, Dark solitons and vortices in $\mathcal{PT}$-symmetric nonlinear media: From spontaneous symmetry breaking to nonlinear $\mathcal{PT}$ phase transitions, Phys. Rev. A **86**, 013808 (2012)

[20] Y. Lumer, Y. Plotnik, M. C. Rechtsman, and M. Segev, Nonlinearly Induced *PT* Transition in Photonic Systems, Phys. Rev. Lett. **111**, 263901 (2013).

[21] J. Yang, Symmetry breaking of solitons in one-dimensional parity-time-symmetric optical potentials, Opt. Lett. **39**, 5547 (2014).

[22] D. A. Zezyulin and V. V. Konotop, Nonlinear modes in the harmonic $\mathcal{PT}$-symmetric potential, Phys. Rev. A **85**, 043840 (2012).

[23] Y. Hadad, A. B. Khanikaev, and A. Alù, Self-induced topological transitions and edge states supported by nonlinear staggered potentials, Phys. Rev. B **93**, 155112 (2016).

[24] D. A. Dobrykh, A. V. Yulin, A. P. Slobozhanyuk, A. N. Poddubny, and Yu. S. Kivshar, Nonlinear Control of

Electromagnetic Topological Edge States, Phys. Rev. Lett. **121**, 163901 (2018).

[25] V. V. Konotop and D. A. Zezyulin, Odd-Time Reversal $\mathcal{PT}$ Symmetry Induced by an Anti-$\mathcal{PT}$-Symmetric Medium, Phys. Rev. Lett. **120**, 123902 (2018).

[26] V. V. Konotop and D. A. Zezyulin, Spectral singularities of odd-$\mathcal{PT}$-symmetric potentials, Phys. Rev. A **99**, 013823 (2019).

[27] L. Ge and H. E. Türeci, Antisymmetric $\mathcal{PT}$-photonic structures with balanced positive- and negative-index materials, Phys. Rev. A **88**, 053810 (2013).

[28] J.-H. Wu, M. Artoni, and G. C. La Rocca, Parity-time-antisymmetric atomic lattices without gain, Phys. Rev. A **91**, 033811 (2015).

[29] V. V. Konotop, D. E. Pelinovsky, and D. A. Zezyulin, Discrete solitons in $\mathcal{PT}$-symmetric lattices, Europhys. Lett. **100**, 56006 (2012).

[30] K. Jones-Smith and H. Mathur, Non-Hermitian quantum Hamiltonians with PT symmetry, Phys. Rev. A **82**, 042101 (2010).

[31] C. M. Bender and S. P. Klevansky, $\mathcal{PT}$-symmetric representations of fermionic algebras, Phys. Rev. A **84**, 024102 (2011).

[32] M. J. Rice and E. J. Mele, Elementary Excitations of a Linearly Conjugated Diatomic Polymer, Phys. Rev. Lett. **49**, 1455 (1982).

[33] C. Hang, G. Huang, and V. V. Konotop, $\mathcal{PT}$ Symmetry with a System of Three-Level Atoms, Phys. Rev. Lett. **110**, 083604 (2013).

[34] J. Sheng, M. Miri, D. N. Christodoulides, and M. Xiao, $\mathcal{PT}$-symmetric optical potentials in a coherent atomic medium, Phys. Rev. A **88**, 041803(R) (2013).

[35] P. Peng, W. Cao, C. Shen, W. Qu, J. Wen, L. Jiang, and Y. Xiao, Anti-parity-time symmetry with flying atoms, Nat. Phys. **12**, 1139 (2016).

[36] Z. Zhang, Y. Zhang, J. Sheng, L. Yang, M. Miri, D. N. Christodoulides, B. He, Y. Zhang, and M. Xiao, Observation of Parity-Time Symmetry in Optically Induced Atomic Lattices, Phys. Rev. Lett. **117**, 123601 (2016).

[37] M. Fleischhauer, A. Imamoglu, and J. P. Marangos, Electromagnetically induced transparency–Optics in coherent media, Rev. Mod. Phys. **77**, 633 (2005).

[38] S. Ghosh, A. R. Bhagwat, C. K. Renshaw, S. Goh, A. L. Gaeta, and B. J. Kirby, Low-Light-Level Optical Interactions with Rubidium Vapor in a Photonic Band-Gap Fiber, Phys. Rev. Lett. **97**, 023603 (2006).

[39] N. V. Corzo, J. Raskop, A. Chandra, A. S. Sheremet, B. Gouraud, and J. Laurat, Waveguide-coupled single collective excitation of atomic arrays, Nature (London) **566**, 359 (2019).

[40] See Supplemental Material at http://link.aps.org/supplemental/ 10.1103/PhysRevA.103.L040202 for technical details of the solutions of the Bloch equation, specific physical parameters of the discussed system, as well as details of the perturbation analysis for nonlinear edge states, which includes Refs. [41–48].

[41] G. S. Agarwal, G. Vemuri, and T. W. Mossberg, Lasing without inversion: Gain enhancement through spectrally colored population pumping, Phys. Rev. A **48**, R4055(R) (1993).

[42] G. Vemuri and D. M. Wood, Lasing without inversion with a fluctuating pump: Gain dependence on pump noise and frequency, Phys. Rev. A **50**, 747 (1994).

[43] C. Hang, D. A. Zezyulin, V. V. Konotop, and G. Huang, Tunable nonlinear parity-time-symmetric defect modes with an atomic cell, Opt. Lett. **38**, 4033 (2013).

[44] C. Hang, D. A. Zezyulin, G. Huang, V. V. Konotop, and B. A. Malomed, Tunable nonlinear double-core PT-symmetric waveguides, Opt. Lett. **39**, 5387 (2014).

[45] A. Yariv and A. P. Yeh, *Photonics: Optical Electronics in Modern Communications*, 6th ed. (Oxford University Press, Oxford, UK, 2007).

[46] G. Agrawal, *Nonlinear Fiber Optics*, 5th ed. (Academic, New York, 2012).

[47] P. Delplace, D. Ullmo, and G. Montambaux, Zak phase and the existence of edge states in graphene, Phys. Rev. B **84**, 195452 (2011).

[48] M. Atala, M. Aidelsburger, J. T. Barreiro, D. Abanin, T. Kitagawa, E. Demler, and I. Bloch, Direct measurement of the Zak phase in topological Bloch bands, Nat. Phys. **9**, 795 (2013).

[49] D. Xiao, M. C. Chang, and Q. Niu, Berry phase effects on electronic properties, Rev. Mod. Phys. **82**, 1959 (2010).

[50] R. Wang, X. Z. Zhang, and Z. Song, Dynamical topological invariant for the non-Hermitian Rice-Mele model, Phys. Rev. A **98**, 042120 (2018).

[51] S. Yao and Z. Wang, Edge States and Topological Invariants of Non-Hermitian Systems, Phys. Rev. Lett. **121**, 086803 (2018).

[52] S. Yao, F. Song, and Z. Wang, Non-Hermitian Chern Bands, Phys. Rev. Lett. **121**, 136802 (2018).

[53] Yu. V. Bludov and V. V. Konotop, Surface modes and breathers in finite arrays of nonlinear waveguides, Phys. Rev. E **76**, 046604 (2007).

[54] Q. E. Hoq, R. Carretero-González, P. G. Kevrekidis, B. A. Malomed, D. J. Frantzeskakis, Yu. V. Bludov, and V. V. Konotop, Surface solitons in three dimensions, Phys. Rev. E **78**, 036605 (2008).

[55] K. Li, D. A. Zezyulin, V. V. Konotop, and P. G. Kevrekidis, Parity-time-symmetric optical coupler with birefringent arms, Phys. Rev. A **87**, 033812 (2013).